

Spatial Characterization for High-Speed Railway Channels Based on Moving Virtual Array Measurement Scheme

Tao Zhou, *Member, IEEE*, Cheng Tao, *Member, IEEE*, Sana Salous, *Senior Member, IEEE*, and Liu Liu, *Member, IEEE*

Abstract—In this letter, spatial channel characterization in high-speed railway (HSR) scenarios is investigated using a moving virtual array measurement approach. Based on the wideband single-antenna measurements conducted on HSR in China and the moving virtual array measurement scheme, 1×3 single-input multiple-output channel impulse responses are generated. Spatial characteristics in the obstructed viaduct and deep cutting scenarios, focusing on angle of arrival, angle spread, and spatial correlation, are analyzed. The obtained results can fulfill the gap of HSR spatial channel models and provide helpful reference for the assessment of HSR multi-antenna technologies.

Index Terms—High-speed railway channel, virtual array, angle of arrival, angle spread, spatial correlation.

I. INTRODUCTION

CHANNEL characterization is the foundation for the research and development of future high-speed railway (HSR) broadband communication systems. Accurate knowledge of spatial characteristics is vital to the modeling of multiple-input multiple-output (MIMO) channels and evaluation of MIMO technologies in HSR scenarios. Reported works on HSR channels have so far been mainly focused on large scale fading, delay and frequency dispersion [1]–[5]. Angular characterization for HSR channels was first presented in [6] where the angle spread (AS) was obtained from single-input multiple-output (SIMO) measurements with relay coverage (RC). Although the well-known WINNER II model [6] includes these angular results into the D2a scenario which is regarded as a kind of fast train scenario, it does not specify the applicable HSR scenarios, e.g., viaduct or cutting. In [7], spatial channel measurements using the direct coverage (DC) scheme were conducted for analyzing the angle of arrival (AOA) and AS information in specific HSR environments

This work was supported by the National Natural Science Foundation of China under Grants 61371070 and 61471030, the Beijing Natural Science Foundation under Grant 4142041, the Fundamental Research Funds for the Central Universities under Grant 2016RC031, and the Open Research Fund through the National Mobile Communications Research Laboratory, Southeast University, under Grant 2014D05.

T. Zhou and L. Liu are with the Institute of Broadband Wireless Mobile Communications, Beijing Jiaotong University, Beijing 100044, China (e-mail: taozhou.china@gmail.com; liuliu@bjtu.edu.cn).

C. Tao is with the Institute of Broadband Wireless Mobile Communications, Beijing Jiaotong University, Beijing 100044, China, and also with the National Mobile Communications Research Laboratory, Southeast University, Nanjing 210096, China (e-mail: chtao@bjtu.edu.cn).

S. Salous is with the School of Engineering and Computing Sciences, Durham University, Durham DH1 3LE, U.K. (e-mail: sana.salous@durham.ac.uk).



Fig. 1. Overview of the obstructed viaduct scenario (left) and deep cutting scenario (right).

including an agricultural area and a hilly district. However, the spatial characteristics derived from the DC measurements embody the effect of scatterers and reflectors inside the train carriage, which cannot represent the realistic angular dispersion in the outdoor propagation environment of HSR. Besides, based on a simple 2×2 RC channel measurement in the HSR viaduct scenario, reference [8] only obtained the spatial correlation results, regardless of the angular characteristics. In fact, performing MIMO channel measurements on HSR is highly difficult due to the waveform repetition frequency (WRF) restriction of conventional channel sounders with the full sequential architecture [9]. It is the lack of MIMO channel data that leads to the huge gap of spatial channel models in HSR scenarios. In this letter, we will employ a moving virtual array measurement scheme [10] to transform the existing single-antenna measurement data into multiple-antenna data. Then we will extract and analyze the spatial characteristics in typical viaduct and cutting scenarios to facilitate MIMO channel modeling and MIMO technology evaluation for the next-generation HSR mobile communication system.

II. MEASUREMENTS

A. Scenario Description

A wideband channel sounder, Propsound, was used to conduct RC channel measurements on Zhengzhou-Xi'an HSR in China [11]. The transmitter (TX) equipped with a vertically polarized dipole antenna is placed near the track to send out an excitation signal. The receiver (RX) is positioned inside the train carriage and employs a special train-mounted antenna, HUBER+SUHNER [12], to collect the test signal. Two typical HSR scenarios, obstructed viaduct and deep cutting scenarios, are chosen in the measurements as shown in Fig. 1. The detailed measurement configuration is listed in Table I.

TABLE I
MEASUREMENT CONFIGURATION

Scenario	Viaduct	Cutting
Measurement frequency /MHz	2350	2350
Transmitted power /dBm	30.8	32.7
Measurement Bandwidth /MHz	50	50
Waveform repetition frequency /Hz	1968.5	1968.5
TX antenna height /m	12.8	13.8
RX antenna height /m	11	3
Distance between TX and railway track /m	92	30
Train velocity /km/h	198	198

For the obstructed viaduct scenario, there are some obvious local scatterers around the viaduct, such as dense trees which are much higher than the train-mounted antenna. These local scatterers will hinder the propagation of radio waves in the TX-RX link and result in serious channel dispersion. The height of TX antenna is not dominant compared to the RX antenna due to the limited test condition. In this case, the effect of shadowing will be further intensified. In contrast, there are few obstacles in the cutting that seems a semi-closed structure with steep walls on both sides of the railway track. However, since the slopes are usually covered by vegetation, they will produce a great deal of extra reflections and scattering. Moreover, the RX is lower than the steep walls leading to a deep cutting scenario which leads to more multipath components [13]. Especially, there exists a cross-bridge used for setting the TX antenna, which could result in short term blockage of the propagation path.

B. Data Processing Based on Moving Virtual Array Measurement Scheme

The snapshot of channel impulse response (CIR) is continuously captured by Propsound at a certain interval. This interval is inversely proportional to the waveform repetition frequency (WRF) that should be at least twice the maximum expected Doppler shift. In the analysis, the used CIR data contain $M = 45108$ snapshots with the time interval of 0.51 ms, corresponding to 22.9 s duration. Each snapshot consists of $L = 254$ multipath taps. Here, the raw CIR is denoted as $h(t, \tau)$, where t and τ are the time and delay, respectively.

In [10], the moving virtual array measurement scheme considering several adjacent snapshots in the moving single-antenna measurement as the multiple-antenna data has been proposed and verified. The neighboring samples of CIR can correspond to several antenna elements which form a virtual uniform line array (ULA) with the direction paralleled to the moving track. To enable this scheme, the fundamental condition is that the channel should be constant in the duration of the samples which are regarded as the equivalent array elements. In other words, the duration should be less than the coherence time of the channel, expressed as

$$(K - 1) \cdot T_{rep} < T_c, \quad (1)$$

where K is the number of equivalent array elements, T_{rep} denotes the time interval of snapshots, and T_c indicates the coherence time.

It is assumed that $T_c = 1/B_d$ [14], where $B_d = 2f_{max}$ is the Doppler spread and f_{max} is the highest Doppler shift. Equation (1) is then rewritten as

$$K < 1 + \frac{1}{2 \cdot f_{max} T_{rep}} = 1 + \frac{1}{2 \cdot \frac{v T_{rep}}{\lambda}}, \quad (2)$$

where v is the moving speed and λ is the wavelength.

According to Equation (2), the maximum number of equivalent array elements is determined by the sampling distance $\Delta d = v T_{rep}$ per wavelength. Substituting the values from Table I into Equation (2), $K < 3.28$, which indicates that the virtual array can support a maximum of three elements. Here, we consider a speed-sensor solution to generate the virtual antenna array and choose $K = 3$ to construct a three-element virtual ULA with the spacing of 0.22λ which is determined by the train velocity and the time interval of CIR. It should be noticing that the train velocity is assumed to keep stable.

The CIR from the TX to the n -th virtual receive element ($n = 1, 2, 3$) is derived by

$$h_n(t, \tau) = h(t_{3m+n}, \tau), \quad m = 0, 1, 2, \dots \quad (3)$$

Finally, the multiple-antenna channel data $\mathbf{h}(t, \tau) = [h_1(t, \tau) \ h_2(t, \tau) \ h_3(t, \tau)]$ are generated, which can be used for the spatial characterization.

III. SPATIAL CHARACTERISTICS

A. Angle of Arrival

The first spatial parameter we focus on is the AoA in azimuth at the RX side. The estimation of signal parameters by the rotational invariance techniques (ESPRIT) algorithm which creates the signal subspace and then extracts the angle information in closed form is capable of analyzing the AOA of the incident wave. By comparing the different ESPRIT algorithms, Unitary ESPRIT is finally chosen because of the lower computational complexity and higher estimation accuracy [15]. For the used Unitary ESPRIT algorithm, there is a limitation that the number of incident waves whose direction can be estimated should be less than the amount of antenna array elements. Since the three-element virtual ULA is employed in the measurements, it can only identify one or two incident waves for each cluster. In this case, it is difficult to analyze the cluster-wise angle information. Here, we concentrate on the global angle parameter which is of interest in the geometric MIMO channel modeling [7].

The Unitary ESPRIT algorithm is applied to the measurement data $\mathbf{h}(t, \tau_l)$ and provides the estimates of AOAs and their respective power associated with the l -th delay. Fig. 2 illustrates the AOA results over 22.9 s measurement period for the strongest cluster in the viaduct and cutting scenarios. The theoretical AOA for the line-of-sight (LOS) condition, as a reference, is also shown in Fig. 2. In [16], the theoretical time-varying AOA is given by

$$\tilde{\varphi}(t) = \arccos \left(\frac{D_s/2 - vt}{\sqrt{D_{min}^2 + (D_s/2 - vt)^2}} \right), \quad 0 \leq t \leq D_s/v, \quad (4)$$

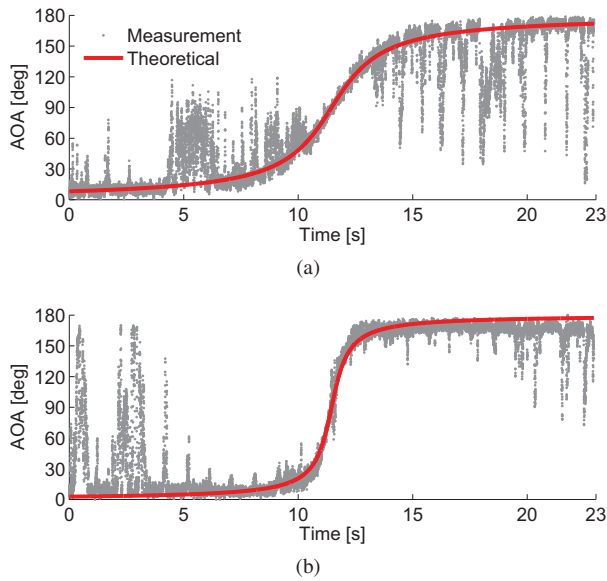


Fig. 2. Time-varying AOA in viaduct (a) and cutting (b) scenarios.

where $D_s/2$ is the initial distance of the train from TX and D_{\min} denotes the distance between TX and railway track. In the measurements, $D_s = 1259.5$ m, $v = 55$ m/s and $D_{\min} = 92$ m and $D_{\min} = 30$ m for the viaduct and cutting scenarios respectively.

It is observed from Fig. 2 that there is a good match between the measurement result and theoretical result with regard to the overall AOA variation tendency. The AOA changes approximately from 0 degree to 180 degree due to the impact of the movement of the train. Since the TX in the cutting scenario is much closer to the railway track, the variation of AOA in the cutting scenario is faster than that in the viaduct scenario when the train passes through the TX. On the other hand, the AOA values in some regions have a larger deviation from the theoretical results. This is because there is no obvious LOS cluster appearing in these regions, e. g., the areas of high dense trees in the viaduct scenario and cross-bridge in the cutting scenario, where the estimated AOA results belong to the non-LOS (NLOS) clusters.

B. Angle Spread

AS is an important parameter which describes the spatial dispersion of multipath channels. The AS is calculated as the root second central moment of power angular spectrum (PAS) which characterizes how much power arrives on average from a certain angle. Based on the extracted AOA and the corresponding power, we can generate the global PAS for each snapshot, denoted as $P_A(t, \varphi)$. Then the time-varying global root mean square (RMS) AS is estimated by

$$\Omega_{\text{RMS}}(t) = \sqrt{\frac{\int [\varphi(t) - \bar{\varphi}(t)]^2 P_A(t, \varphi) d\varphi}{\int P_A(t, \varphi) d\varphi}}, \quad (5)$$

where $\bar{\varphi}(t)$ is the averaged AOA, expressed as

$$\bar{\varphi}(t) = \frac{\int \varphi(t) P_A(t, \varphi) d\varphi}{\int P_A(t, \varphi) d\varphi}. \quad (6)$$

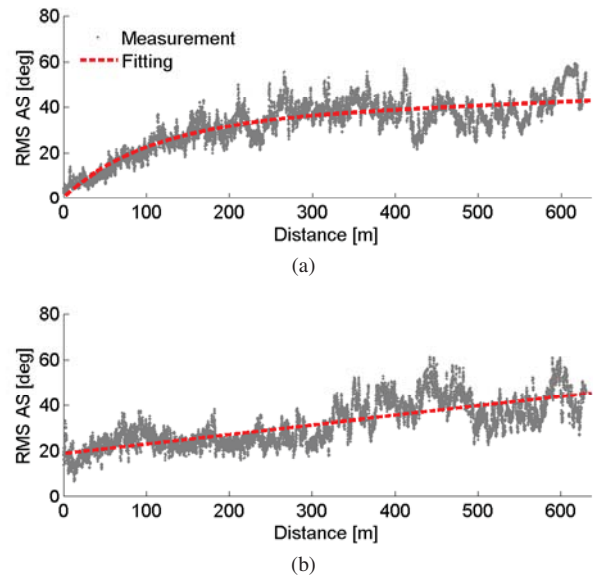


Fig. 3. Distance-dependent RMS AS in viaduct (a) and cutting (b) scenarios.

It is worth noticing that due to the limited measurement bandwidth, the number of resolvable multipath components is constrained, which will affect the accuracy of the RMS AS. To improve the accuracy of the RMS AS, we should either increase the measurement bandwidth or employ more antennas in the measurement.

The relation between the channel parameter and the distance is always of interest in channel characterization [17]. Here, $\Omega_{\text{RMS}}(t)$ is transformed into the RMS AS as a function of the distance, expressed as $\Omega_{\text{RMS}}(d)$. It is noted that the distance represents the relative horizontal distance between the transceivers, and $\Omega_{\text{RMS}}(d)$ indicates the averaged RMS AS in two segments (the western half and the eastern half of the route).

Fig. 3 shows the distance-dependent RMS AS results in the obstructed viaduct and deep cutting scenarios. It can be seen that the RMS AS experiences a gradual growth with the distance in both scenarios. This means that more clusters which cause the larger AS can be identified as the distance increases. To describe the variation of RMS AS, we employ a double exponential function and a linear function to fit the RMS AS curves using the least square (LS) method, expressed as

$$\bar{\Omega}_{\text{RMS}}(d) = \begin{cases} 34.19e^{0.00035d} - 33.65e^{-0.0095d}, & \text{viaduct} \\ 0.041d + 18.78, & \text{cutting} \end{cases} \quad (7)$$

Finally, a distance-dependent statistical model for the RMS AS is proposed as

$$\Omega_{\text{RMS}}(d) = \bar{\Omega}_{\text{RMS}}(d) + x\sigma, \quad (8)$$

where $\bar{\Omega}_{\text{RMS}}(d)$ denotes the mean value of the RMS AS, $\sigma = 11.6$ deg and $\sigma = 10.1$ deg indicate the standard deviations in the viaduct and cutting scenarios respectively, and x represents a zero-mean Gaussian variable with unity standard deviation.

A detailed comparison of the statistic RMS AS results for the obstructed viaduct, deep cutting, WINNER D2a, agricultural area and hilly district scenarios is shown in Table II.

TABLE II
COMPARISON OF THE STATISTIC AS RESULTS IN DIFFERENT SCENARIOS

Scenario	Obstructed Viaduct	Deep Cutting	WINNER D2a [6]	Agricultural Area [7]	Hilly District [7]
Coverage scheme	RC	RC	RC	DC	DC
10% /deg	15.15	20.8	21.3	-	-
50% /deg	34.7	29.9	30.4	-	-
90% /deg	45.6	46.3	45.9	-	-
Mean /deg	32.7	31.9	32.5	75	60

It is observed that the mean value of RMS AS measured in the RC scheme is much smaller than the result obtained in the DC scheme. This confirms that the indoor environment of the train causes additional scattering and reflecting waves, leading to the larger AS. For the RC scheme, although 10% values of RMS AS in the obstructed viaduct scenario are lower than those in the deep cutting and WINNER D2a scenarios and 50% values in the obstructed viaduct scenario are higher than the results in the other two scenarios, there are similar mean values and 90% values in the three scenarios. This means that the obstructed viaduct scenario could have an equivalent propagation effect to the deep cutting scenario as a whole and the undefined WINNER D2a scenario probably belongs to a kind of obstructed viaduct or deep cutting scenarios.

C. Spatial Correlation

Spatial correlation (SC) between different antenna elements at both ends of the individual link is a key parameter of MIMO channels. In order to extract the SC, we transform the wideband data into the narrowband data $\mathbf{h}(t)$ by taking the complex sum of $\mathbf{h}(t, \tau)$ over the delay domain. The SC coefficient between the virtual elements is calculated by

$$\rho_{12(3)}(t) = \frac{E[h_1(t)h_{2(3)}^*(t)]}{\sqrt{Var[h_1(t)]Var[h_{2(3)}(t)]}}, \quad (9)$$

where $E[\cdot]$ and $Var[\cdot]$ denote the expected value and the variance of $[\cdot]$, respectively, and $h_{2(3)}^*(t)$ indicate the complex conjugation of $h_{2(3)}(t)$.

Fig. 4 depicts the cumulative distribution function (CDF) results of ρ_{12} and ρ_{13} with the antenna spacing of $\delta = 0.22\lambda$ and $\delta = 0.44\lambda$ in the viaduct and cutting scenarios. It can be found that 95% values of SC are higher than 0.8. The strong SC is mainly due to the smaller antenna spacing ($\delta < 0.5\lambda$) in the measured scenarios. It can be also seen that the SC in the viaduct scenario decreases more as the antenna spacing increases, which means the antenna spacing has a stronger impact on SC in the obstructed viaduct scenario compared to the deep cutting scenario.

IV. CONCLUSION

This letter presents the spatial channel characteristics in HSR obstructed viaduct and deep cutting scenarios, based on 1×3 multi-antenna channel data obtained by the wideband SISO measurements and the moving virtual array measurement scheme. It shows that the measured AOA has a reasonable consistency with the theoretical result. As for the RMS

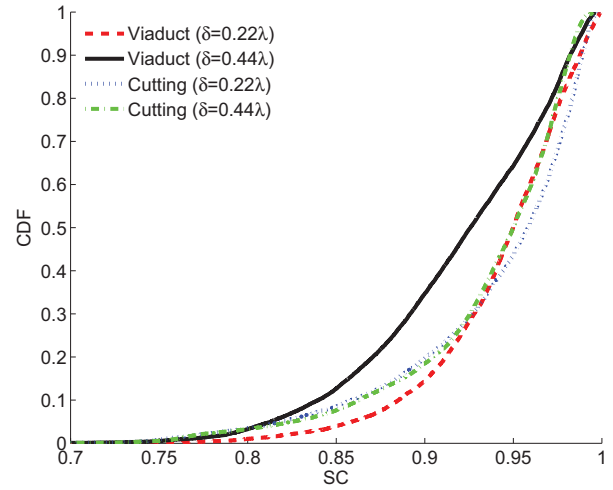


Fig. 4. CDFs of SC in the viaduct and cutting scenarios.

AS, a distance-dependent statistical model is proposed. In addition, the SC for the two scenarios are analyzed in the case of different antenna spacings. These results will provide useful information for channel modeling and performance evaluation for future HSR MIMO systems.

REFERENCES

- [1] B. Ai, X. Cheng, T. Kürner, Z. D. Zhong, K. Guan, R. S. He, L. Xiong, D. W. Matolak, D. G. Michelson, and C. B. Rodriguez, "Challenges toward wireless communications for high-speed railway," *IEEE Tran. Intell. Transp.*, vol. 15, no. 5, pp. 2143-2158, Oct. 2014.
- [2] B. Ai, K. Guan, M. Rupp, T. Kürner, X. Chen, X. F. Yin, Q. Wang, G. Y. Ma, Y. Li, L. Xiong, and J. W. Ding, "Future Railway Traffic Services Oriented Mobile Communications Network," *IEEE Commun. Mag.*, vol. 53, no. 10, pp. 78-85, Oct. 2015.
- [3] C. X. Wang, A. Ghazal, B. Ai, Y. Liu, and P. Fan, "Channel measurements and models for high-speed train communication systems: a survey," *IEEE Commun. Surveys Tuts.*, vol. 18, no. 2, pp. 974-987, May 2016.
- [4] L. Liu, C. Tao, J. Qiu, H. Chen, L. Yu, W. Dong, and Y. Yuan, "Position-based modeling for wireless channel on high-speed railway under a viaduct at 2.35 GHz," *IEEE J. Sel. Area. Commun.*, vol. 30, no. 4, pp. 834-845, May 2012.
- [5] R. He, Z. Zhong, B. Ai, and J. Ding, "An empirical path loss model and fading analysis for high-speed railway viaduct scenarios," *IEEE Antennas Wireless Propag. Lett.*, vol. 10, pp. 808-812, Aug. 2011.
- [6] P. Kyösti et al., "WINNER II channel models part II radio channel measurement and analysis results," 2007.
- [7] R. Parviainen, P. Kyösti, and Y. Hsieh, "Results of high speed train channel measurements," European Cooperation in the Field of Scientific and Technical Research, Tech. Rep., 2008.
- [8] Q. Wang, C. Xu, M. Zhao, and D. Yu, "Results and analysis for a novel 2×2 channel measurement applied in LTE-R at 2.6 GHz," *Proc. IEEE WCNC*, 2014, pp. 177-181.
- [9] T. Zhou, C. Tao, S. Salous, L. Liu, and Z. H. Tan, "Channel sounding for high-speed railway communication systems," *IEEE Commun. Mag.*, vol. 53, no. 10, pp. 70-77, Oct. 2015.

- [10] B. Chen, Z. Zhong, B. Ai, and D. G. Michelson, "Moving virtual array measurement scheme in high-speed railway," *IEEE Antennas Wireless Propag. Lett.*, vol. 15, pp. 706-709, Mar. 2016.
- [11] T. Zhou, C. Tao, L. Liu, and Z. H. Tan, "Ricean K-factor measurements and analysis for wideband high-speed railway channels at 2.35 GHz," *Radioengineering*, vol. 23, no. 2, pp. 578-585, Jun. 2014.
- [12] Sencity Rail Antenna: 1399.17.0039 HUBER+SUHNER data sheet, HUBER+SUHNERAG RF Industrial, 2010.
- [13] R. He, Z. Zhong, B. Ai, and J. Ding, "Propagation measurements and analysis for high-speed railway cutting scenario," *Electronics Letters*, vol. 47, no. 21, pp. 1167-1168, Oct. 2011.
- [14] A. Goldsmith, *Wireless Communications*. Cambridge, U.K.: Cambridge Univ. Press, 2005.
- [15] M. Haardt and J. A. Nossek, "Unitary ESPRIT: how to obtain increased estimation accuracy with a reduced computational burden," *IEEE Trans. Signal Processing*, vol. 43, no. 5, pp. 1232-1242, May 1995.
- [16] 3GPP, TS 36.104 V9.3.0 3rd Generation Partnership Project; Technical Specification Group Radio Access Network; Evolved Universal Terrestrial Radio Access (e-utra); Base Station (BS) radio transmission and reception (Release 9), 2010.
- [17] C. Oestges, D. Vanhoenacker-Janvier, and B. Clerckx, "Wide-band SIMO 1×2 measurements and characterization of outdoor wireless channels at 1.9 GHz," *IEEE Trans. Veh. Technol.*, vol. 53, no. 4, pp. 1190-1202, May 2004.